Urban Rail Transit (2022) 8:267–285
https://doi.org/10.1007/s40864-022-00173-y

http://www.urt.cn/

ORIGINAL RESEARCH PAPERS

Influence of Structural Types of CRTS I Plate-Type Ballastless Track on Aerodynamic Characteristics of High-Speed Train

Liming Du[1] · Chenjie Bian[2] · Peng Zhang[1]

Received: 14 June 2022 / Revised: 28 July 2022 / Accepted: 8 August 2022 / Published online: 28 September 2022

Abstract In order to improve the running quality of trains on a ballastless track, the influence of the CRTS I ballastless track with different structures (flat-type and frame-type tracks) is investigated with respect to the aerodynamic characteristics of high-speed trains. In the present paper, the aerodynamic force changes on the head, middle, tail, and whole car of the high-speed train were studied under two conditions, with crosswind and without crosswind, and the influence of different crosswind speeds (10, 15, 20, 25, 30 m/s) on the aerodynamic force of the train was analyzed. The pressure and flow field distribution characteristics were also studied, and the reasons for the different aerodynamic characteristics of different track structures and trains running in different wind environments were analyzed, respectively. The results indicate that the ballastless track structure obviously influences the aerodynamic characteristics of the high-speed train. When there is no natural wind, compared with the flat track, the frame track reduces the drag and lateral forces of the train but increases the lift force. The frame track causes the drag force of the whole vehicle to decrease slightly (the maximum ratio is 2.15%), the lift force increases significantly (the maximum ratio is 12.55%), and the lateral force obviously decreases (the maximum ratio is 52.43%). The lift and lateral forces of the middle car are most affected, which is because the frame structure changes the vortex motion state of the middle car. Compared with the flat track, the drag force of each car on the frame track is reduced under the crosswind; the lift force of each car is increased, and the maximum increase in the lift force of the head, middle, and tail cars is 5.60%, 2.55%, and 3.63%, respectively; the lateral force of the tail car increases greatly at a wind speed of 15 m/s, reaching 6.84%. Due to the existence of the frame structure, the space under the vehicle increases, resulting in a decrease in the airflow rate and an increase in local pressure, which leads to changes in the train's aerodynamic force. Meanwhile, the train's aerodynamic change under the crosswind is smaller than that when there is no wind.

Keywords High-speed train · Ballastless track · Aerodynamic performance · Flow field characteristics

✉ Liming Du
dlm@djtu.edu.cn

Chenjie Bian
18015305009@163.com

1 School of Locomotive and Rolling Stock Engineering, Dalian Jiaotong University, Dalian 116028, Liaoning, China

2 School of Civil Engineering, Dalian Jiaotong University, Dalian 116028, Liaoning, China

Communicated by Liang Gao.

1 Introduction

With the continuous improvement in high-speed train infrastructure construction technology, ballastless tracks are gradually replacing ballasted tracks on most lines, becoming the most widely used track type. A ballastless track has the advantages of good smoothness and stability, which are beneficial for high-speed train operation. However, there are many types of ballastless tracks, and the influence of the various structural types on the aerodynamic characteristics of high-speed trains differs greatly, which will affect the running stability of high-speed trains. Among these types, the flat type and the frame type have been widely used track structures. In addition, in different wind environments, the aerodynamic response and flow field characteristics of high-speed trains running on ballastless tracks are also different. Under special conditions, this is likely to affect the operational safety of high-speed trains. In order to ensure the safety and stability of high-speed trains and passenger comfort, it is necessary to study the aerodynamic response and flow field characteristics of high-speed trains running on different types of ballastless tracks in different wind environments.

In the past, scholarly research has focused mostly on the aerodynamic performance of trains running on ballasted tracks. Xiao [1] and García et al. [2] studied the influence of the ballasted track on the flow field characteristics under the train. Ding [3] studied the flow field characteristics on the surface of the ballast bed, the flow characteristics under the train, the aerodynamic characteristics of ballast particles, and the influence of the ballast bed structure on the flying ballast, using the wind tunnel test and CFD method. However, he adopted a shortmarshalling train model. Zhang et al. [4] established a high-speed train model consisting of nine cars and studied the aerodynamic characteristics of the train when it ran on flat ground, 3 m embankment, 6 m embankment, and viaduct under a crosswind. However, the ballastless track was not considered in this model, and the influence of the ballastless track on the aerodynamic performance of the train was ignored. Li et al. [5] designed a wind tunnel test including a vehicle-bridge-track system and studied the flow structure and far-field noise of the high-speed train on a ballastless track. The lateral vortices are typical unsteady flow structures, and the flow near the ground is a chaotic flow. Some scholars [6, 7] have studied the influence of different wind environments on the aerodynamic performance of trains.

Regarding the research on ballastless tracks, most scholars have focused on their structural deformation [8], coupled vibration [9], and dynamic performance [10–12]. Lin et al. [13] studied the coupled vibration of the under-rail structure when high-speed trains meet at constant speed on the ballastless track structure of a bridge. He focused on the lateral and vertical dynamic responses of the meeting trains and concluded that the horizontal dynamic response of meeting wind pressure was greater than the vertical. Chen et al. [14] studied the vibration response of trains under different ballastless tracks and only analyzed the mechanical characteristics. Jiang et al. [15] studied the effect of the uneven settlement of the subgrade on the dynamic response of the track system. Meanwhile, some scholars have also researched the fatigue damage of ballastless tracks [16–18].

According to the above analysis, various studies have investigated the aerodynamic performance of trains under ballasted tracks, the aerodynamic performance of trains under different wind conditions, and the structural deformation, coupled vibration, and fatigue damage of ballastless tracks. In the future, ballastless track will replace ballasted track on most lines. However, there are few studies about the influence of ballastless tracks with different structures on the aerodynamic performance of high-speed trains, which will affect the running stability of high-speed trains and the comfort of passengers. Therefore, the research in the present paper is of great significance. This article focuses on the influence of changes in the ballastless track structure on the aerodynamic characteristics of high-speed trains. Using the steady calculation method, we analyzed the influence of two different China Railway Track System CRTS I ballastless tracks on the aerodynamic characteristics of high-speed trains under no natural wind and crosswind environments. Additionally, the reasons for the differences in the aerodynamic characteristics are analyzed from the perspective of flow field characteristics.

2 Numerical Model and Calculation Method

2.1 Train and Track Model

A three-dimensional (3D) geometric model of a three-section China Railway High-speed (CRH) train is established. The train adopts a simplified model, which has a smooth surface and only retains the bogie structure. Meanwhile, it can be simplified into three-section marshaling, which includes the head, middle, and tail car [19]. The lengths of the head, middle, and tail cars are 25.64, 25.12, and 25.64 m, respectively, and the total length (L) is 76.4 m; the width (D) is 3.26 m, and the height (H) is 3.89 m. The geometric model of the train is shown in Fig. 1. The distance between the wheel tread and the track is 0.02 m, and the space height between the vehicle and the track is about 0.35 m.

In this paper, we adopt a CRTS I ballastless track [16] when comparing the influence of two types of ballastless track structures on the aerodynamic characteristics of high-speed trains. The track is divided into two types: flat and frame type. The dimensions of the two types of track slabs are exactly the same except for the structural form. The length of the two track plates is 4.93 m, the width is 2.4 m,

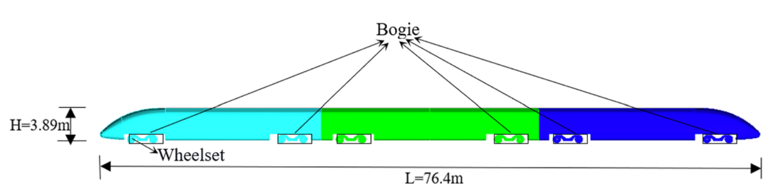

Fig. 1 Train model

and the height is 0.19 m. The width of the track base is 3 m and the height is 0.3 m. The height of the rail is 0.176 m when the structure of the rail support is ignored. The dimensions of the frame-type track slab are 2.8 m length, 0.8 m width, and 0.19 m depth. The size information for flat-type and frame-type ballastless track models is shown in Fig. 2.

2.2 Computational Domain

When there is no natural wind, the size of the calculation domain is 276.4 (3.62 L) × 60 (18.41 D) × 30 m (7.71 H). The length and height of the calculation domain under crosswind are as same as the condition of no natural wind. In order to fully develop the air on the leeward side of the train under the crosswind, the longitudinal length of the front area of the train is greater than ten times the width of the train, and the longitudinal length of the rear area is at least twice the total length of the train. Thus, the width is 150 m (46 D) and the distance between the centerline of the track and the entrance of the crosswind is 50 m (15.34 D). The computational domain size conforms to the blocking ratio theory holding that the ratio of the projected area of the experimental model on the experimental air duct section to the air duct section is less than 5%. The calculation domain and boundary conditions of no natural wind and crosswind are shown in Fig. 3. The air density is 1.225 kg/m^3, and the air viscosity is 1.7894×10^{-5} N s/m^2.

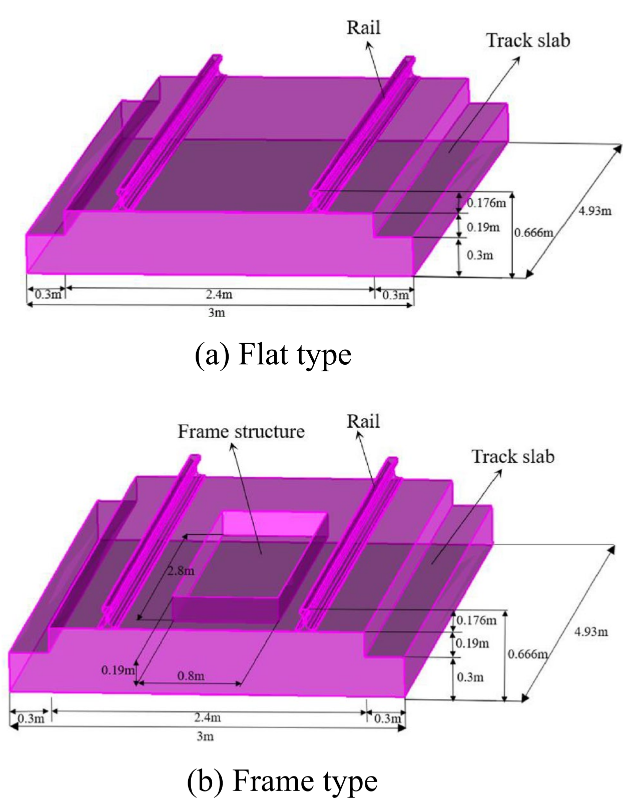

Fig. 2 Flat and frame ballastless track

2.3 Computational Grid and Numerical Methods

The calculation area is divided by hybrid grids, and the grids of the car body and the bogie are encrypted. The maximum grid size of the car body and the bogie is 0.1 and 0.05 m, respectively. The wall surface function method is used at the wall. The height of the first layer is 0.3 mm, such that the y+ meets the requirement of $50 < y+ < 180$ [20, 21]. The growth ratio is 1.2, the total number of layers is 4, and the total number of grids is about 8.5 million. The grids are shown in Fig. 4.

The numerical simulation was carried out by the commercial software Ansys Fluent. A sliding wall is set on the track wall to simulate the relative motion between the train and the track. The turbulence model selects the RNG $k-\varepsilon$ two-equation turbulence model [22, 23]. The calculation method adopts the SIMPLE [Semi-Implicit Method for Pressure Linked Equations] algorithm and uses the second-order upwind style to discretize the computational domain to solve the three-dimensional, steady, incompressible turbulent flow around the high-speed train.

2.4 Numerical Model Validation

As shown in Fig. 5, the aerodynamic forces of the train include drag, lift, and lateral forces along the three coordinate axes, namely, F_x, F_y, and F_z. When the aerodynamic force is decomposed according to the direction of the wind, the drag force is parallel to the incoming flow direction, and the lift and lateral forces are perpendicular to the incoming flow direction. The corrsponding modifications are in the file “Response to editiors”.

$$F_x = \frac{1}{2}\rho AV^2 C_x \tag{1}$$

$$F_y = \frac{1}{2}\rho AV^2 C_y \tag{2}$$

$$F_Z = \frac{1}{2}\rho AV^2 C_Z \tag{3}$$

The formula for drag, lift, and lateral forces are shown above. In the formula, A is the reference area (the maximum cross-section area of the car body), V is the reference speed (the running speed of the train), C_x is the drag force coefficient, C_y is the lift force coefficient, and C_Z is the lateral force coefficient [24].

Fig. 3 Computational domain model and boundary conditions

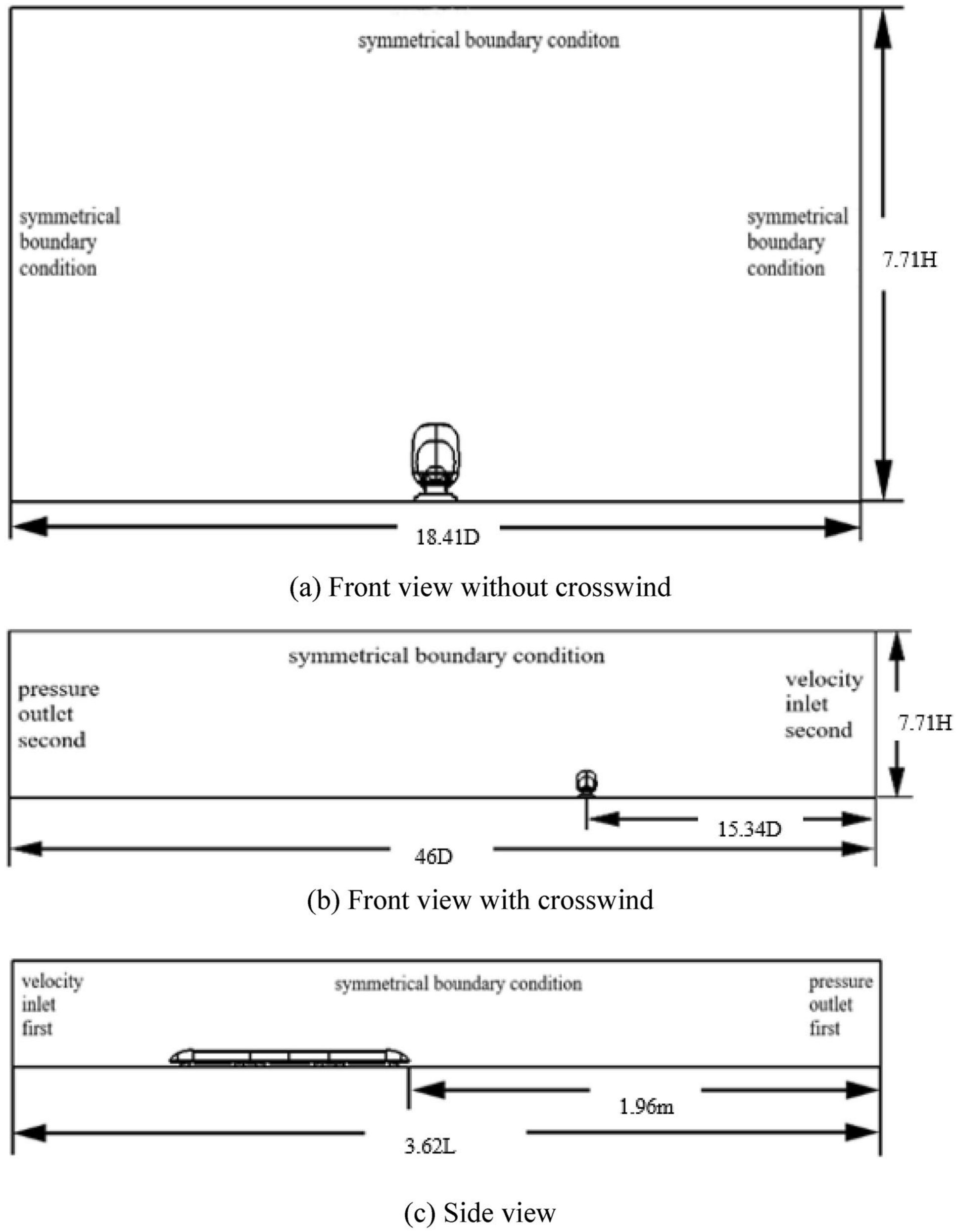

Generally, the numerical results must be compared with actual vehicle tests, wind tunnel tests, or existing reliable research data to verify their credibility. However, there are few relevant wind tunnel experiments on high-speed trains running on the CRTS I ballastless track with different structures. Therefore, the simulation conditions of open space and straight roads shown in the literature [25] were used to verify the numerical simulation in this article, and the wind tunnel test results were compared to verify the feasibility of the numerical model and method. The reduction ratio of the CRH train and the wind tunnel is 1:8 in the literature. The same reduction model was used in the present article, with a cross-sectional dimension of 8 m × 6 m and a length of 16 m. The incoming flow velocity is 60 m/s, and the airflow angle is 3°. The numerical simulation test verification model is shown in Fig. 6.

The comparison of the drag, lift, and lateral force coefficients of the whole car from the wind tunnel test [25] and the numerical simulation is shown in Table 1. Table 1 shows that the drag, lift, and lateral force coefficient of the whole car differs by about 8.68, 9.86, and 4.95%, respectively. The deviation is minimal, and the error may be caused by the difference between the numerical model and the wind tunnel test model. This indicates that the numerical model and method used in the present article are feasible.

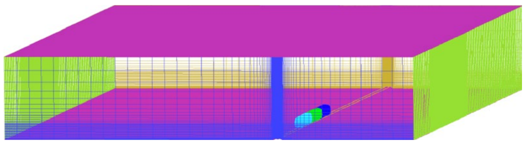

(a) Calculation domain grid

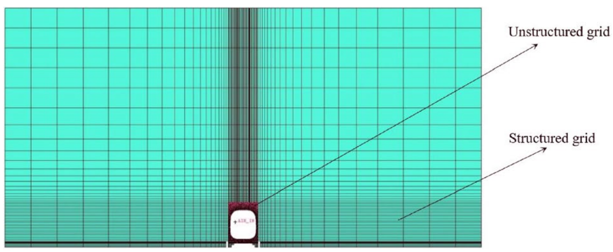

(b) Calculation domain section grid

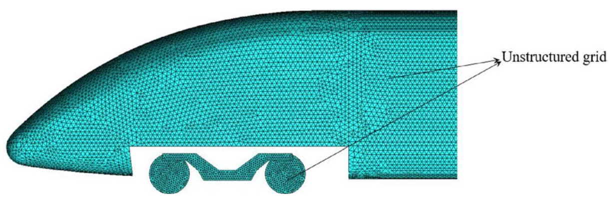

(c) Car-body surface grid

Fig. 4 Calculation domain and body surface grid

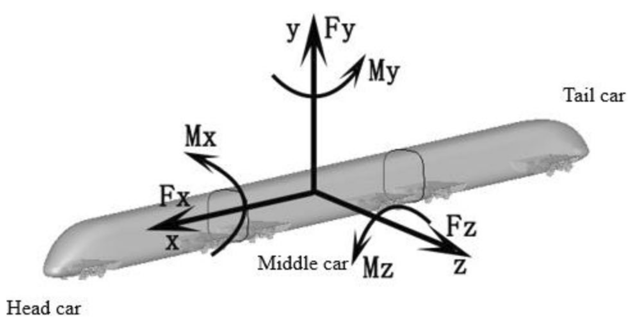

Fig. 5 Schematic diagram of aerodynamic forces

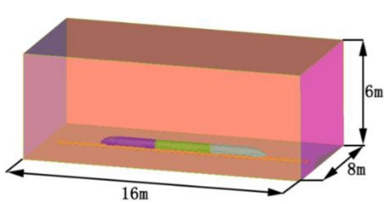

Fig. 6 Numerical simulation test verification model

Table 1 Comparison of the wind tunnel test and numerical results

	Test value	Simulation value	Deviation (%)
Vehicle drag coefficient C_x	0.5018	0.4582	−8.68
Vehicle drag coefficient C_y	0.2333	0.2563	9.86
Vehicle drag coefficient C_z	0.2604	0.2733	4.95

2.5 Grid Independence Verification

As shown in Fig. 7, a total of three sets of grids were selected for independent verification.

Among them, the total number of Mesh 1 is about 6 million, that of Mesh 2 is about 8.5 million, and of Mesh 3 is about 11.25 million. The drag, lift, and lateral force of the head and whole car on the frame track are taken to verify the grid independence under the condition without crosswind. It can be seen that the aerodynamic forces from Mesh 1, 2, and 3 show good agreement, and the maximum deviation is within 10%. In addition, we verified the mesh independence of the other working conditions. The results show that the errors generated by the three groups of mesh are all within 10%. Therefore, Mesh 2 is used for the subsequent investigations.

3 Calculation Results and Analysis

3.1 The Influence of the Ballastless Track Structure on the Aerodynamic Force of the Train Under the Condition of No Natural Wind

When there is no natural wind, the train runs on ballastless tracks with different structures at different speeds. The train speed is between 200 and 400 km/h, and 50 km/h is taken as an interval to obtain five sets of speeds. The aerodynamic data of the train are shown below.

Figure 8 shows a comparison of the drag force of the train on the flat and frame tracks. From the perspective of the whole car drag force, the frame type changes the train drag force slightly compared with the flat type. The reduction percentage of the whole car drag force at different speeds is 2.15, 1.94, 1.78, 1.74, and 1.90%, respectively, and the maximum reduction percentage is only 2.15% [26]. It can be seen that the difference in the influence between these two kinds of track structures on the whole car drag force is relatively small. From the perspective of each car's drag force, the frame type is associated with a significant reduction in the drag force of the head car compared with the flat type. The drag force of the head car is reduced by 5.68, 5.81, 5.87, 5.99, and 6.26%, respectively. The drag force of the middle

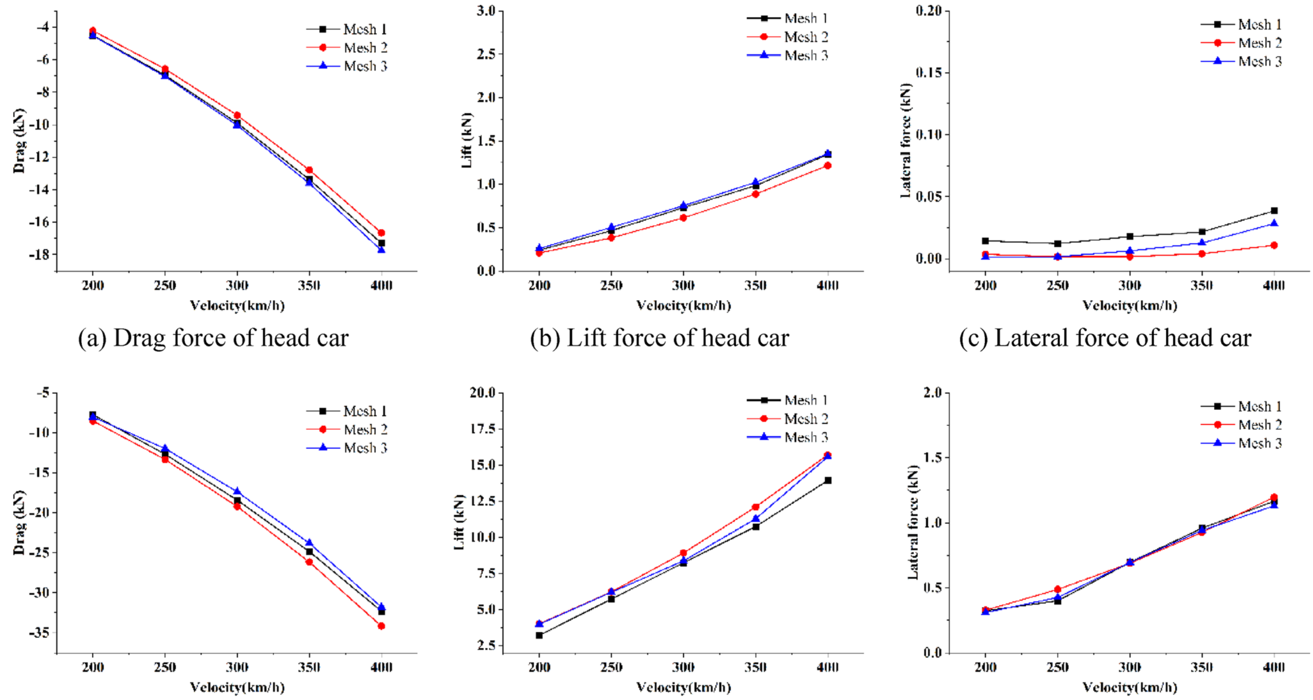

(a) Drag force of head car (b) Lift force of head car (c) Lateral force of head car

(d) Drag force of whole car (e) Lift force of whole car (f) Lateral force of whole car

Fig. 7 Grid independence verification

and tail cars increases slightly. This is because when the head car passes the frame track for the first time, it is affected by the bottom frame, resulting in a reduction in drag force. It can be seen that the drag force of the whole car is mostly affected by the decrease in the drag force of the head car, and the frame track is associated with a relative reduction in the drag force of the train.

Figure 9 shows the comparison of the train lift force of the flat and frame track. It can be seen from the figure that, compared with the flat type, the lift force of the head car under the frame track is reduced by 73.64, 68.80, 64.82, 62.11, and 59.74%, respectively, while the lift force of the middle car rises sharply, changing the direction of the train lift force. But from the perspective of the lift force value alone, it is also reduced, and only the lift force of the tail car increases. As a result, the lift force of the whole vehicle increased by 12.55, 10.59, 9.10, 8.33, and 7.88%, respectively. When the train is on the frame track, there is a certain space under the car, which is filled by the airflow. The bottom airflow will lift the train, increasing the lift force. Therefore, it is necessary to control the size of the frame in the actual engineering. From the view of the three cars, the lift force reduction is largest for the head car, but the lift force increase in the whole car is mainly due to the directional change in the lift force of the middle car.

Figure 10 shows the comparison of the train lateral forces on the flat and frame tracks. Compared with the flat track, the lateral force of the head car increases when the speed is less than 300 km/h, and when the opposite is true, it decreases. But the lateral force of the head car is very small, so the impact on the lateral force of the whole car is very small. The lateral force of the middle car has increased, but the direction has also changed, from positive to negative. At the same time, the lateral force of the tail car is also increasing. However, from the results of the lateral force on the whole vehicle, it can be seen that the lateral force is greatly reduced, and it is mostly affected by the directional change in the lateral force on the middle car. The reduction percentage of the lateral force on the whole car is 46.67, 50.51, 51.42, 51.61, and 52.43%, respectively. It can be seen from the above analysis that the frame track can effectively reduce the lateral force of the train.

3.2 The Influence of the Ballastless Track Structure on the Pressure Distribution Around the Train When There is No Natural Wind

For the two track structures, the lift and lateral forces on the train are significantly different. We analyzed the pressure distribution around the train when it runs at the speed of 350 km/h. The position of the section is shown in Fig. 11. The number from 1 to 6 is the direction from the head car to the tail car, and the numbers are H1, H2, M3, M4, T5, and T6, respectively.

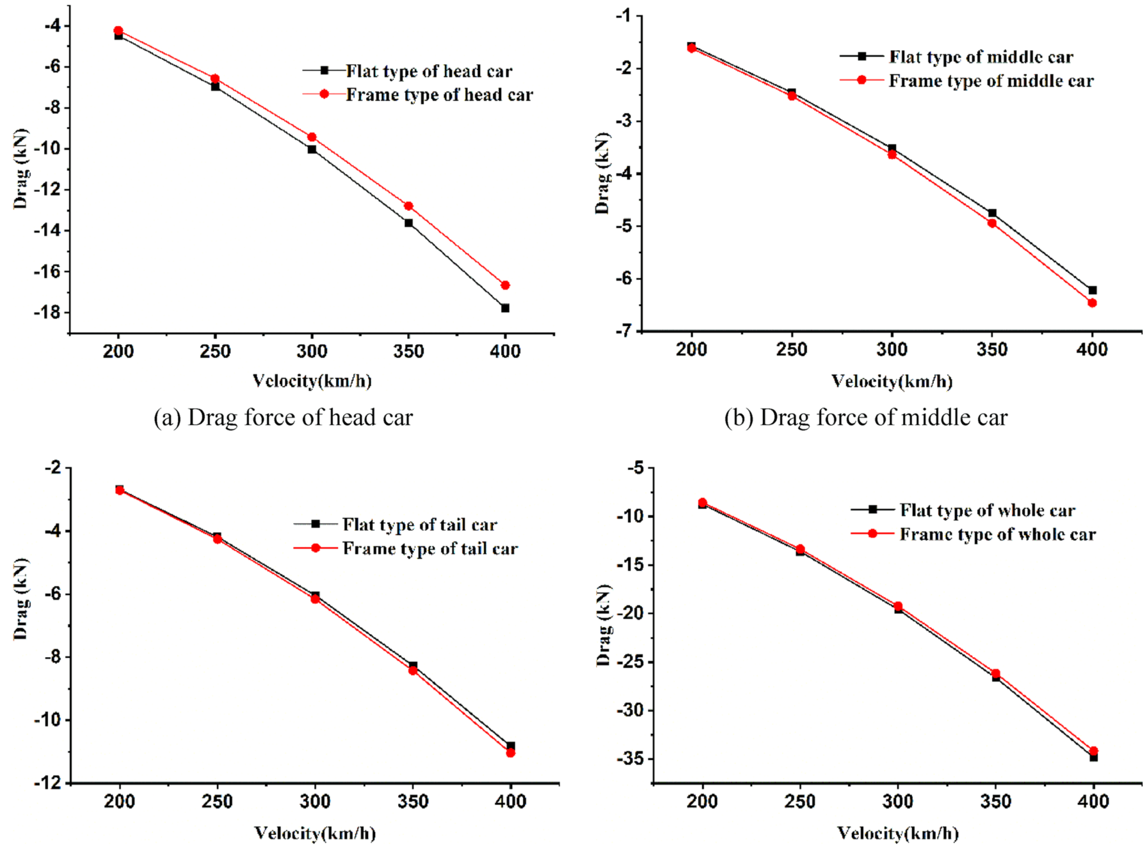

(a) Drag force of head car (b) Drag force of middle car

(c) Drag force of tail car (d) Drag force of whole car

Fig. 8 Comparison of train drag between flat and frame tracks

On the frame track, the bogie center section is divided into two positions: not in the frame structure and in the frame structure. Therefore, in the analysis, sections H1, M3, and T5 are not in the frame structure, and sections H2, M4, and T6 in the frame structure are separated and compared with the sections of the flat track.

Figure 12 shows the pressure distribution around the train body at the H1, M3, and T5 sections. At the H1 section of the head car, the pressure distribution of the two track structures is basically the same, indicating that the frame track structure has a very limited influence on the H1 section of the head car. At the M3 section of the middle car and T5 section of the tail car, however, the pressure distribution around the car body has changed significantly. At the M3 section, the pressure on both sides of the train on the frame track has increased. The underbody pressure near the bogie changes from negative to positive. At the T5 section of the tail car, under the flat track, the left and right sides of the bogie are affected by the center of positive pressure and negative pressure, respectively, and the pressure distribution on both sides of the car body is also affected, while the bogie center of the frame track is mainly affected by negative pressure. Meanwhile, the distribution of positive and negative pressure centers on both sides of the car body is completely opposite that of the flat track.

Figure 13 shows the pressure distribution around the train body at the H2, M4, and T6 sections. At the H2 section of the head car, the undercarriage has a higher positive pressure on the flat track, while the undercarriage of the frame track is completely affected by the negative pressure. This indicates that the frame structure has a large impact on the pressure field under the vehicle. The design department can consider optimizing the size of the frame structure to reduce the pressure under the car, thereby improving the aerodynamic response of the train on the track. In combination with the fact that there is no significant change in the undercarriage pressure from the H1 section, the substantial reduction in the head car lift force is greatly affected by the substantial decrease in the bottom pressure at the H2 section. At the same time, the pressure on both sides of the car body also decreases substantially with the influence of the negative pressure under the car, so the lateral force on the train also decreases. However, due to the symmetrical distribution of the pressure on both sides of the head car, the lateral force

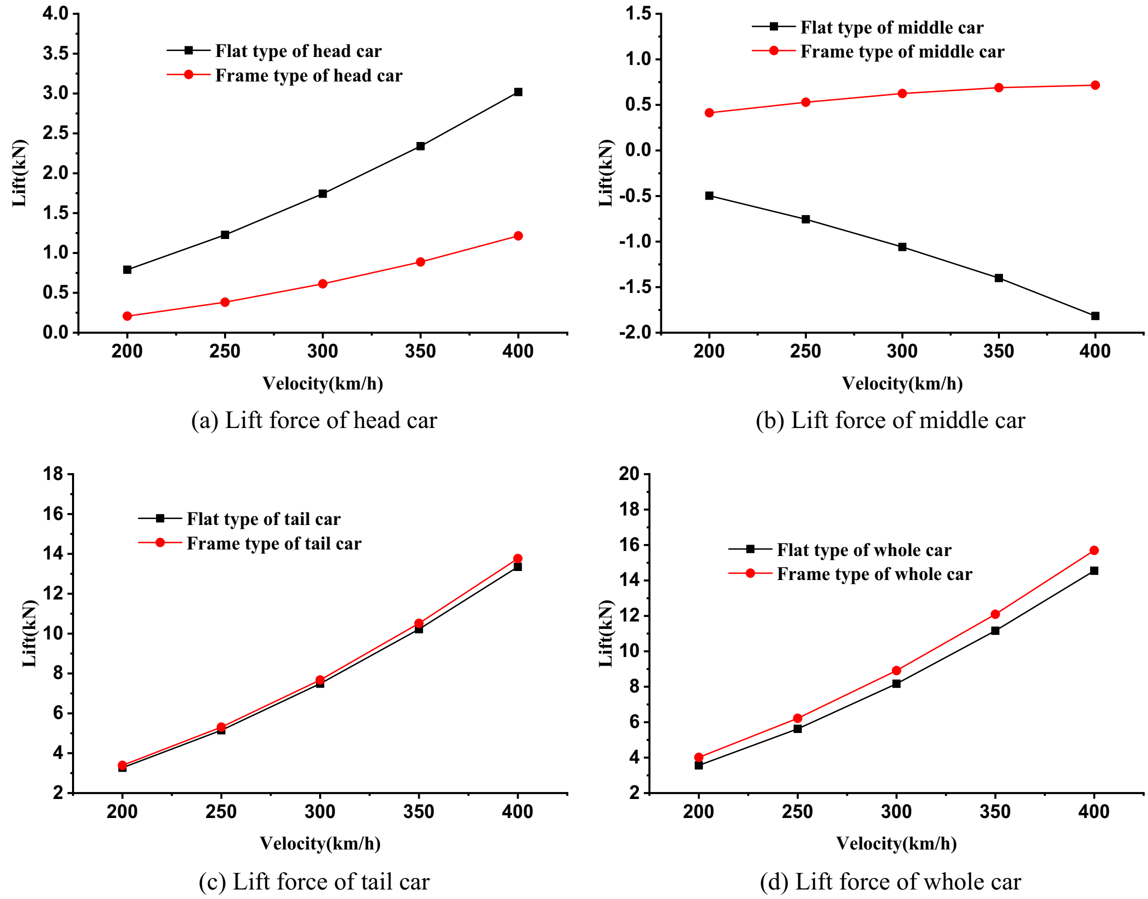

(a) Lift force of head car
(b) Lift force of middle car
(c) Lift force of tail car
(d) Lift force of whole car

Fig. 9 Comparison of train lift between flat and frame track

of the head car is very small, making the influence of the change of the lateral force not obvious.

In the M4 section of the middle car, the pressure change regulation around the car body is basically the same as in the bottom of the car, except that with the change in pressure value, the frame track will affect the pressure of the partial area under the car, but the effect is small. According to the pressure distribution of the M3 and M4 sections of the middle car, the bottom of the car body on the frame track is affected by positive pressure from the M3 section, which is the main reason for the change in the middle car lift from negative to positive. However, the pressure changes on the two sides of the car body in the two sections will not cause a directional change in the lateral force on the train, indicating that the area that has the greatest impact on the lateral force of the middle car is not at the bogie.

At the T6 section of the tail car, the pressure around the car body is roughly equivalent and symmetrically distributed. The pressure under the car is negative, but there is a certain increase in the negative pressure under the car body of the frame track. It can be seen from the T5 and T6 sections that the lateral force of the train on the frame track has increased, which is greatly affected by the position change in the positive and negative pressure centers on both sides of the car body of the T5 section.

3.3 The Influence of the Ballastless Track Structure on the Flow Field Distribution Around the Train When There is No Natural Wind

The following is an analysis of the different reasons for the flow field distribution around the following two types of track structures.

Figure 14 shows the flow field distribution at the H1, M3, and T5 sections. It can be seen from the H1 section that the scroll structure under the car is basically the same, and the position here is less affected by the frame track, so there is no significant change in the pressure distribution of this section on the two track structures. At the H1 section, the pressure spreads from the car body surface to the surroundings, and the streamline also flows to the surroundings. At the M3 and T5 sections, the pressure spreads from bottom to top, and the streamlines also flow to the top. At the bottom and back of the car body, the pressure distribution is

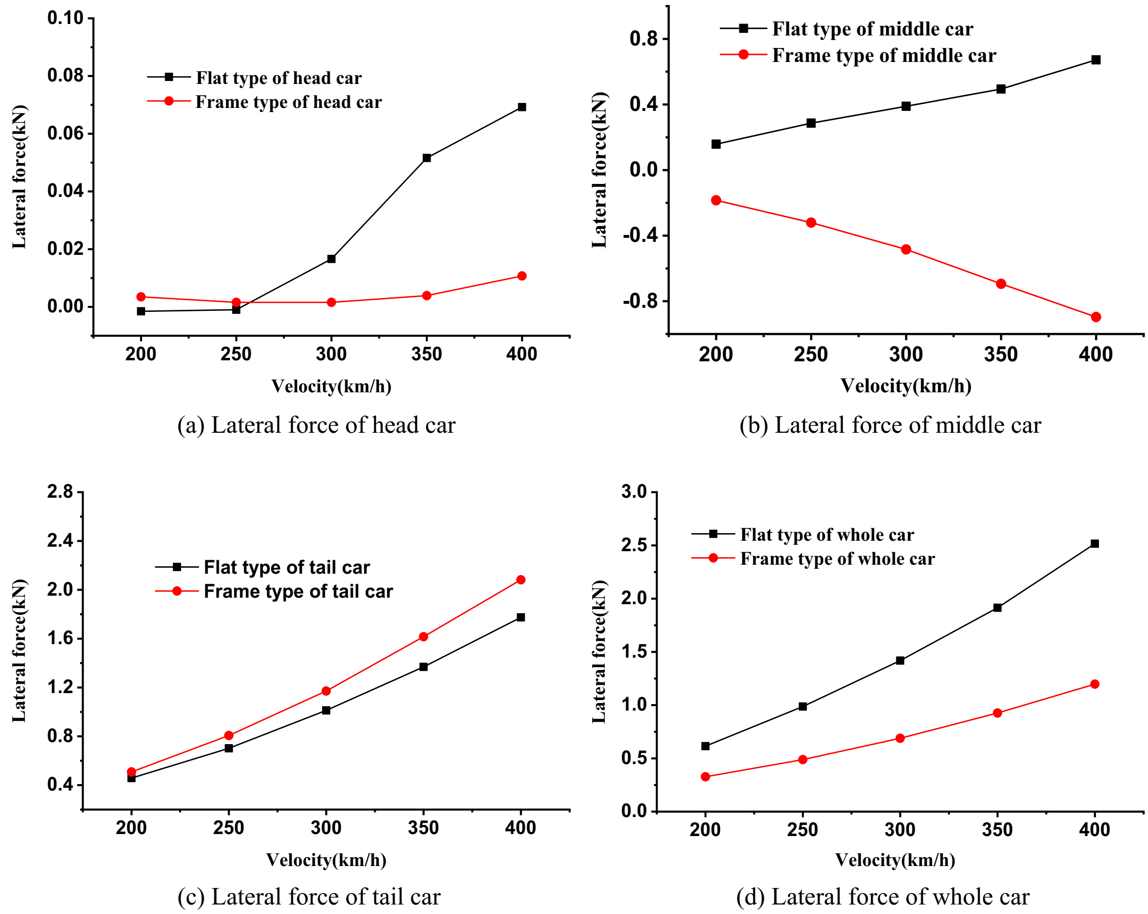

Fig. 10 Comparison of the lateral forces of trains on flat and frame tracks

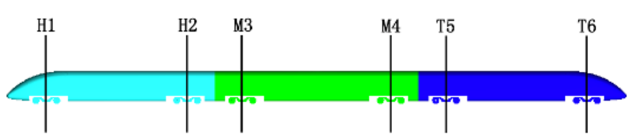

Fig. 11 Section position

uneven, resulting in backflows and vortices. On the frame track of the M3 section, it can be found that there are vortices on both sides of the bogie. At the center of the bogie, there is no other vortex generated except the vortex at the rail. Combined with the pressure distribution from the M3 section, it can be seen that the vortex on the left side of the car body of the frame track is dissipating, and the vortex on the right side is generating. The lower airflow velocity of the frame track results in higher pressure around the car body than on the flat track. The flat track is mainly affected by the dissipative vortex under the car. The airflow velocity is faster, which causes the pressure under the vehicle to be more strongly affected by the negative pressure. At the T5 section, the vortex is generated at the left corner of the car body on the flat track, forming a positive pressure center, while the vortex at the right corner dissipates to form a negative pressure center. The pressure changes on both sides of the car body are affected by the two pressure centers. It can be seen that the generation of vortices will form positive pressure centers, and the dissipation of vortices will form negative pressure centers. Under the frame track, the vortex at the left side of the car body is dissipating, and the airflow velocity in the vortex center is high. Under the influence of this vortex, the pressure on the left side of the bogie is negative, while the higher positive pressure on the right side of the car body is caused by the speed drop due to the airflow around the corner of the car body [27–29].

Figure 15 shows the flow field distribution at the H2, M4, and T6 sections. Under the frame track of the H2 section, the vortex center in the center of the vehicle bottom diverts airflow to the surroundings. From the perspective of pressure distribution, the vehicle bottom is the central area of negative pressure. The pressure gradually increases from the bottom to both sides of the car body, indicating that the vortex at the center of the car bottom is dissipating. The airflow dissipated by the vortex still maintains a high airflow

Fig. 12 Pressure distribution at H1, M3, and T5 sections

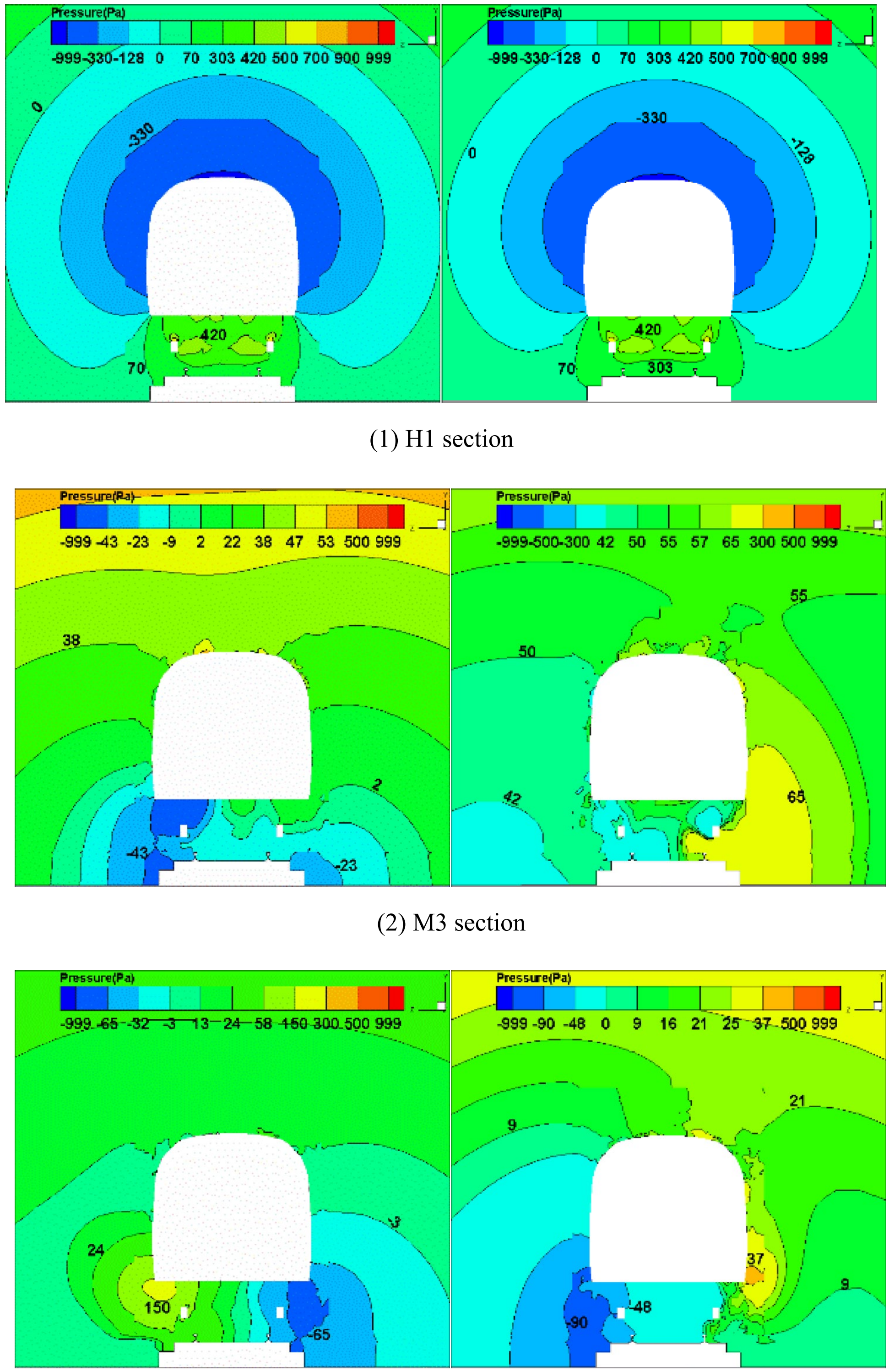

(1) H1 section

(2) M3 section

(3) T5 section

(a) Flat type (b) Frame type

velocity, which results in the negative pressure center. The vortex motion state on either side of the car body has no major influence on the flow field around the vehicle body. In the M4 section, under the two track structures, the air flows in from the left side of the car body and flows out from the right side. Multiple vortices are generated when the air flows

Fig. 13 Pressure distribution at H2, M4, and T6 sections

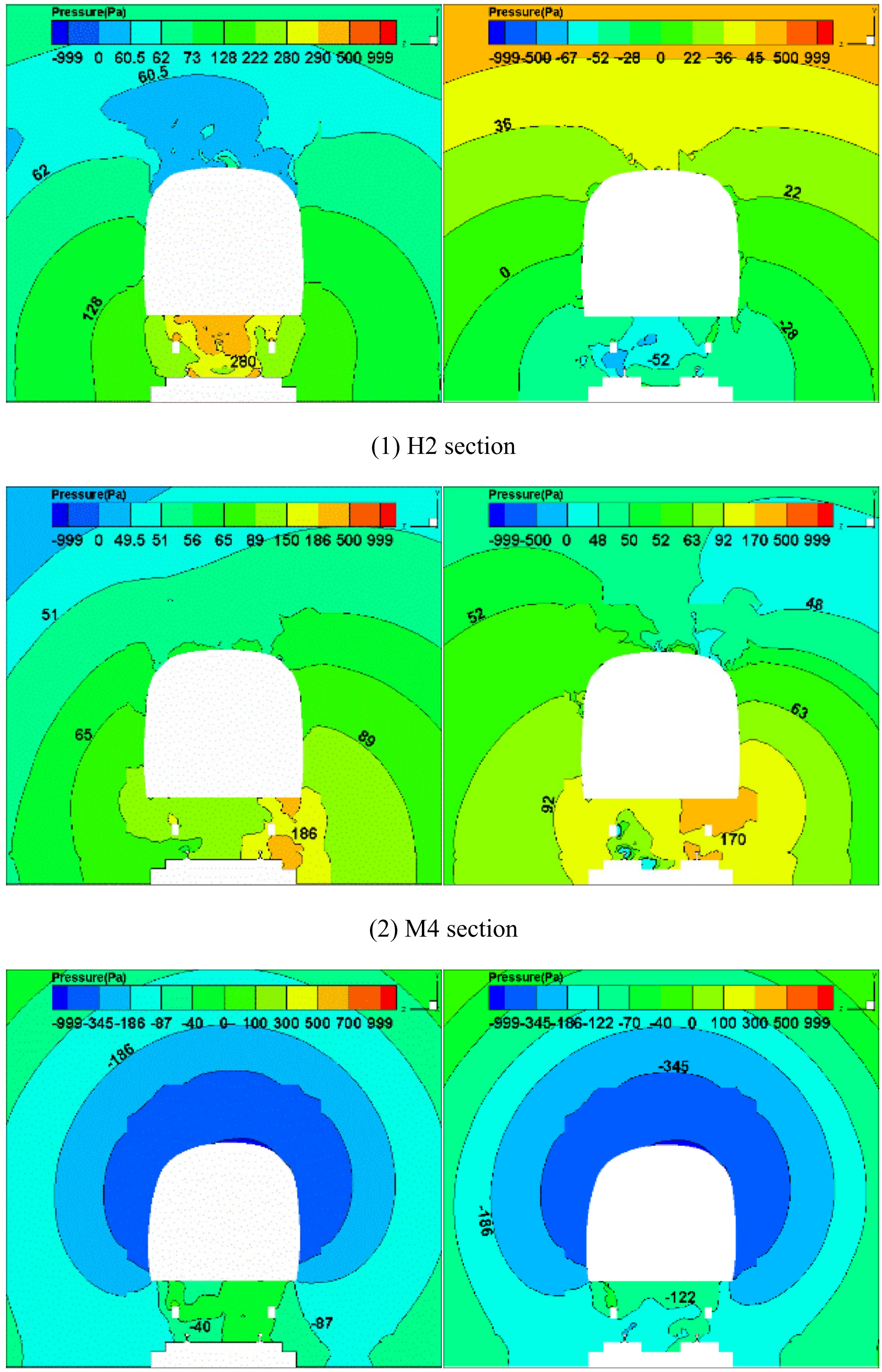

(1) H2 section

(2) M4 section

(3) T6 section

(a) Flat type (b) Frame type

through the vehicle's bottom, so the pressure distribution in this section is roughly the same. The flow field distribution around the car body of the T6 section is exactly the same. Under the frame track, the airflow from the center of the vehicle bottom radiates to the bogie, and the airflow on both sides of the track also flows to the vehicle bottom and forms

Fig. 14 Flow field distribution at H1, M3, and T5 sections

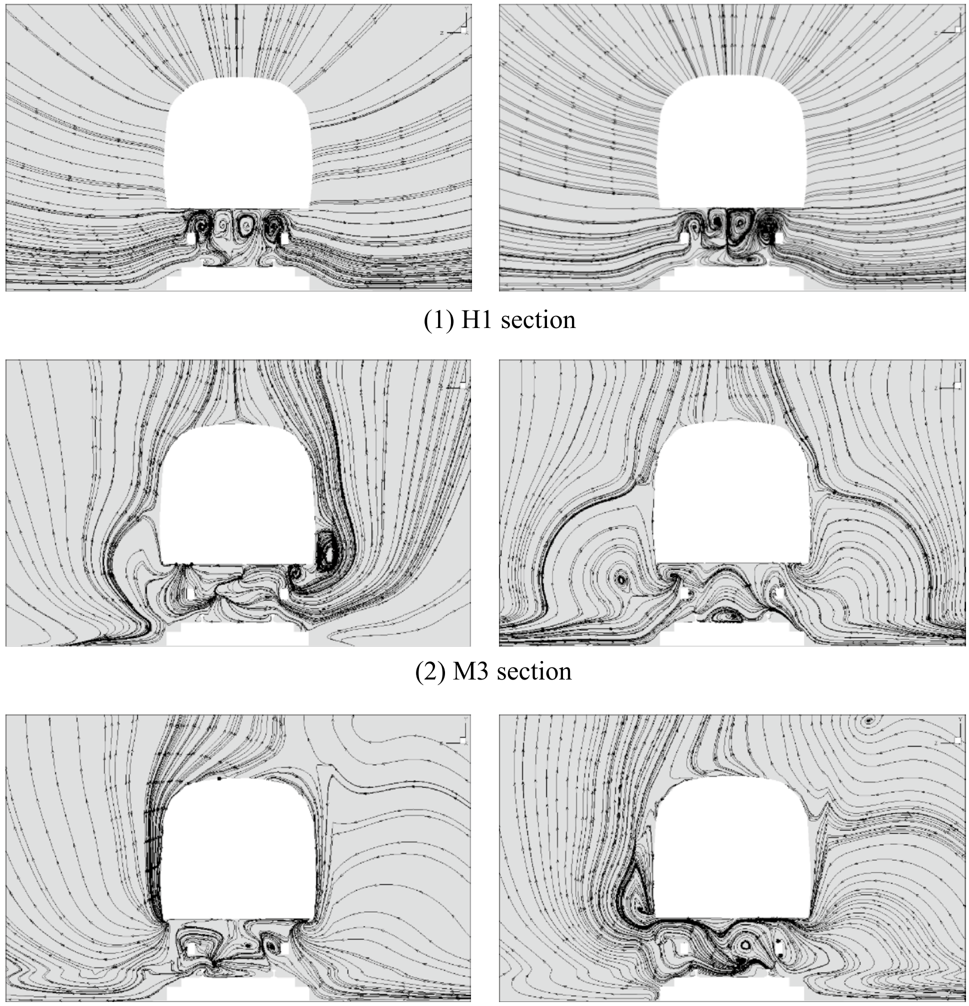

(1) H1 section

(2) M3 section

(3) T5 section

(a) Flat type (b) Frame type

a vortex on the inside of the track. Many vortices are generated near the frame under the flat track, and the influence of the flow field distribution on the pressure distribution cannot be clearly seen.

3.4 The Influence of the Ballastless Track Structure on the Train Aerodynamic Force Under a Crosswind

Because the train aerodynamic changes in the two track structures are not particularly obvious under crosswinds, the difference between the two cannot be intuitively compared using the line graph method. Therefore, we compared the data directly, and the comparison results are shown in the following tables.

Tables 2, 3, and 4 compare the aerodynamic forces of the following two types of track structures. From the drag force data, in addition to individual data, the three cars' drag force of frame type decreases compared with the flat type, but the drag force reduction percentage is very small. The maximum drag force reduction percentage of the three cars at the head, middle, and tail is 0.27, 1.45, and 1.33%, respectively. When the wind speed is 20 m/s or below, the drag force of the head car is least affected by the track structure, and the middle and the tail cars are the most affected. When the wind speed is above 20 m/s, the difference is significantly reduced [30]. Therefore, adjusting the structure and size of the frame can be considered to further reduce the train drag force in the following research.

From the data on lift force, the frame track has a relatively obvious impact on the train lift force, and the lift force of each car is increasing. The maximum lift force increase of the head, middle, and tail cars is 5.60, 2.55, and 3.63%, respectively. The maximum increase in the lift force of the head and tail cars occurred at a wind speed of 10 m/s, while the middle car reached a maximum at a wind speed

Fig. 15 Flow field distribution at H2, M4, and T6 sections

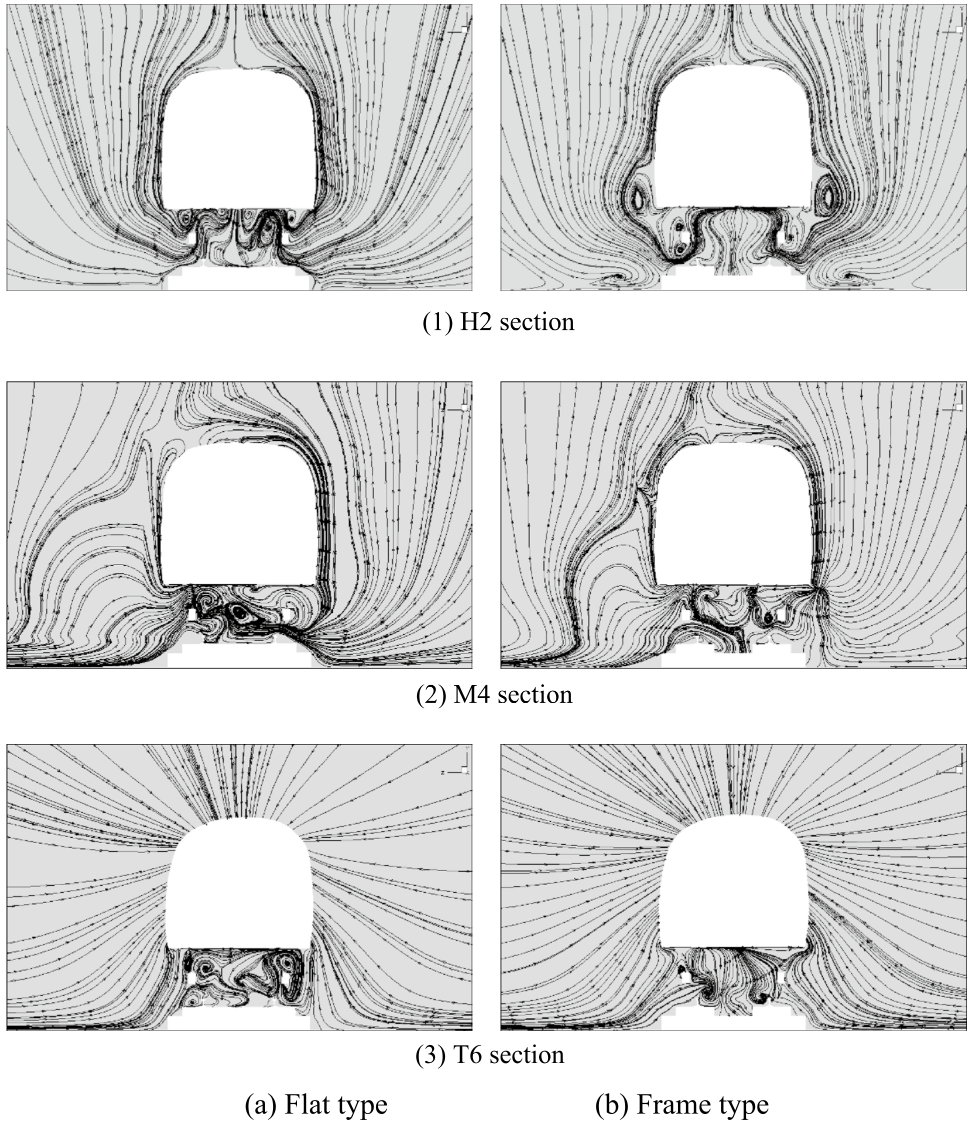

Table 2 Comparison of the drag of trains under flat and frame tracks

Wind speed (m/s)	Drag force (kN)								
	Head car		Change percentage (%)	Middle car		Change percentage (%)	Tail car		Change percentage (%)
	Flat type	Frame type		Flat type	Frame type		Flat type	Frame type	
10	−52.74	−52.93	0.36	−17.28	−17.03	−1.45	−16.63	−16.42	−1.26
15	−65.64	−65.57	−0.11	−25.54	−25.20	−1.33	−30.57	−30.20	−1.21
20	−76.58	−76.37	−0.27	−34.95	−34.66	−0.83	−39.89	−39.36	−1.33
25	−85.79	−85.64	−0.17	−43.77	−43.69	−0.18	−41.48	−41.61	0.31
30	−93.18	−93.06	−0.13	−51.21	−51.19	−0.04	−37.80	−37.74	−0.16

of 30 m/s. Based on the above analysis, the frame track will increase the train lift force. Therefore, high-speed rail operators can consider using trains with heavier body and wheel weights to run on the frame tracks.

From the lateral force data, the difference in the lateral force between the three cars under the two track structures is basically small, less than 1%. Compared with the flat track, the lateral force of the head car under the frame track is

Table 3 Comparison of lift of trains under flat and frame tracks

Wind speed (m/s)	Lift force (kN)								
	Head car		Change percentage(%)	Middle car		Change percentage(%)	Tail car		Change percentage(%)
	Flat type	Frame type		Flat type	Frame type		Flat type	Frame type	
10	52.34	55.27	5.60	94.89	96.70	1.91	114.75	118.91	3.63
15	122.10	125.94	3.14	211.35	214.31	1.40	233.65	239.62	2.56
20	222.71	229.61	3.10	372.31	378.39	1.63	355.75	363.74	2.25
25	354.42	363.73	2.63	554.26	567.51	2.39	446.64	461.11	3.24
30	516.90	527.21	1.99	733.47	752.16	2.55	505.85	518.75	2.55

Table 4 Comparison of the lateral force of trains under flat and frame tracks

Wind speed (m/s)	Lateral force (kN)								
	Head car		Change percentage (%)	Middle car		Change percentage (%)	Tail car		Change percentage (%)
	Flat type	Frame type		Flat type	Frame type		Flat type	Frame type	
10	100.53	100.36	−0.17	53.64	53.16	−0.89	1.46	1.45	−0.68
15	164.74	164.02	−0.44	99.85	99.21	−0.64	14.77	15.78	6.84
20	241.33	240.22	−0.46	153.42	153.22	−0.13	30.02	31.33	4.36
25	331.58	330.14	−0.43	203.06	204.18	0.55	41.94	42.21	0.64
30	434.68	433.82	−0.20	243.58	245.44	0.76	50.19	49.99	−0.40

decreasing. At a wind speed of 20 m/s, the maximum reduction percentage is 0.46%. The increased lateral force of the train is mainly caused by the crosswind. When the head car passes the frame track under the crosswind, part of the airflow will stay in the frame, thereby weakening the crosswind effect on the head car and reducing the lateral force of the head car. When the wind speed is 20 m/s and below, the lateral force of the middle vehicle decreases, and at a higher wind speed, the lateral force starts to increase. The maximum decrease is 0.89% at a wind speed of 10 m/s, and the maximum increase is 0.76% at a wind speed of 30 m/s. The lateral force of the tail car increases greatly at a wind speed of 15 m/s, reaching 6.84%, and then gradually decreases with the increase in wind speed. Therefore, compared with the flat track, the safety of the tail car running on the frame track under the crosswind is worthy of more worth attention. In the area near the track, operators can consider installing windbreaks to reduce the crosswind impact. At speeds of 10 and 30 m/s, the lateral force of the tail car decreases, with maximum reduction of 0.68% at 10 m/s.

3.5 The Influence of the Ballastless Track Structure on the Pressure Distribution Around the Train Under a Crosswind

From the train aerodynamic force analysis of the two track structures under the crosswind, the train lift force is greatly affected. Therefore, at a crosswind speed of 15 m/s, we analyzed the pressure distribution of the central section of each bogie, and the selection position of the section and analysis method is the same as the condition of no natural wind.

Figure 16 shows the pressure distribution at the H1, M3, and T5 sections of the two track structures under the crosswind. It can be seen from the figure that there is no significant difference in the pressure distribution between the frame track and the flat track. The pressure near the bogie decreases slightly, and the pressure distribution on the windward side of the car body is slightly affected. There is an obvious difference when only within the influence range of each pressure center on the leeward side of the car body, which has a certain influence on the lateral force reduction of the train [31, 32].

Figure 17 shows the pressure distribution at the H2, M4, and T6 sections of the two track structures under the crosswind. There is an obvious change in the pressure distribution of the H2 and T6 sections. The pressure of the frame track under the vehicle at the H2 section is significantly increased. The pressure increase of the head car caused an obvious increase in the head car's lift force, which has a major impact on the lift force change of the head car. The pressure center on the windward and leeward sides of the car body also increases significantly. The pressure decreases at the underbody frame and increases at the upper corner of the leeward side of the car at the T6 section. These pressure changes will

Fig. 16 Pressure distribution at H1, M3, and T5 sections

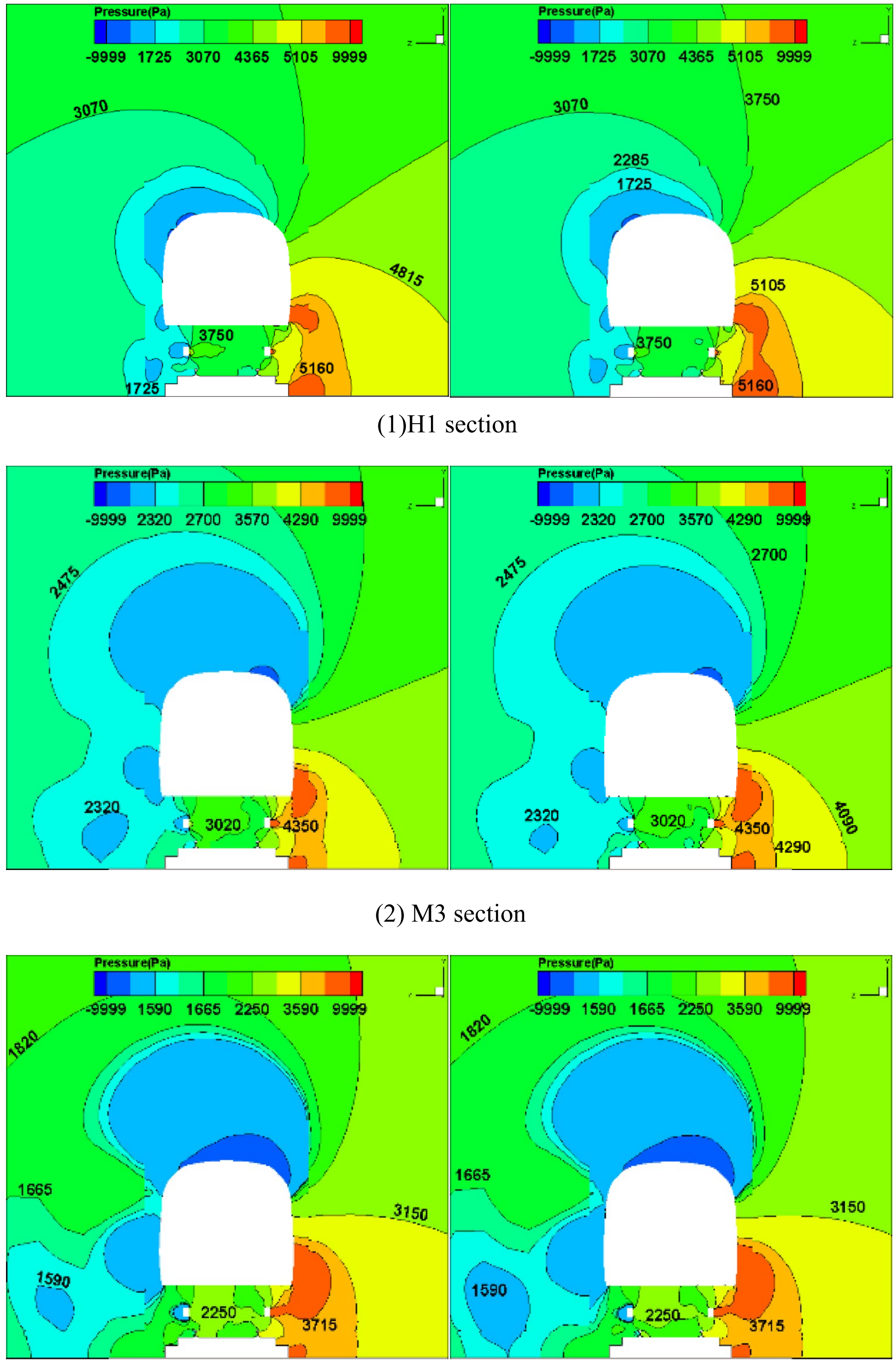

(1)H1 section

(2) M3 section

(3) T5 section

(a) Flat type (b) Frame type

cause the lift force of the tail car to decrease. From the view of lift data, the lift force of the tail car increases, indicating that the position that plays a major role in the change of the lift force of the tail car is not at the tail car bogie. In the M4 section of the middle car, there is still no obvious pressure change under the car or on either side of the car body.

Fig. 17 Pressure distribution at the H2, M4, and T6 Sections

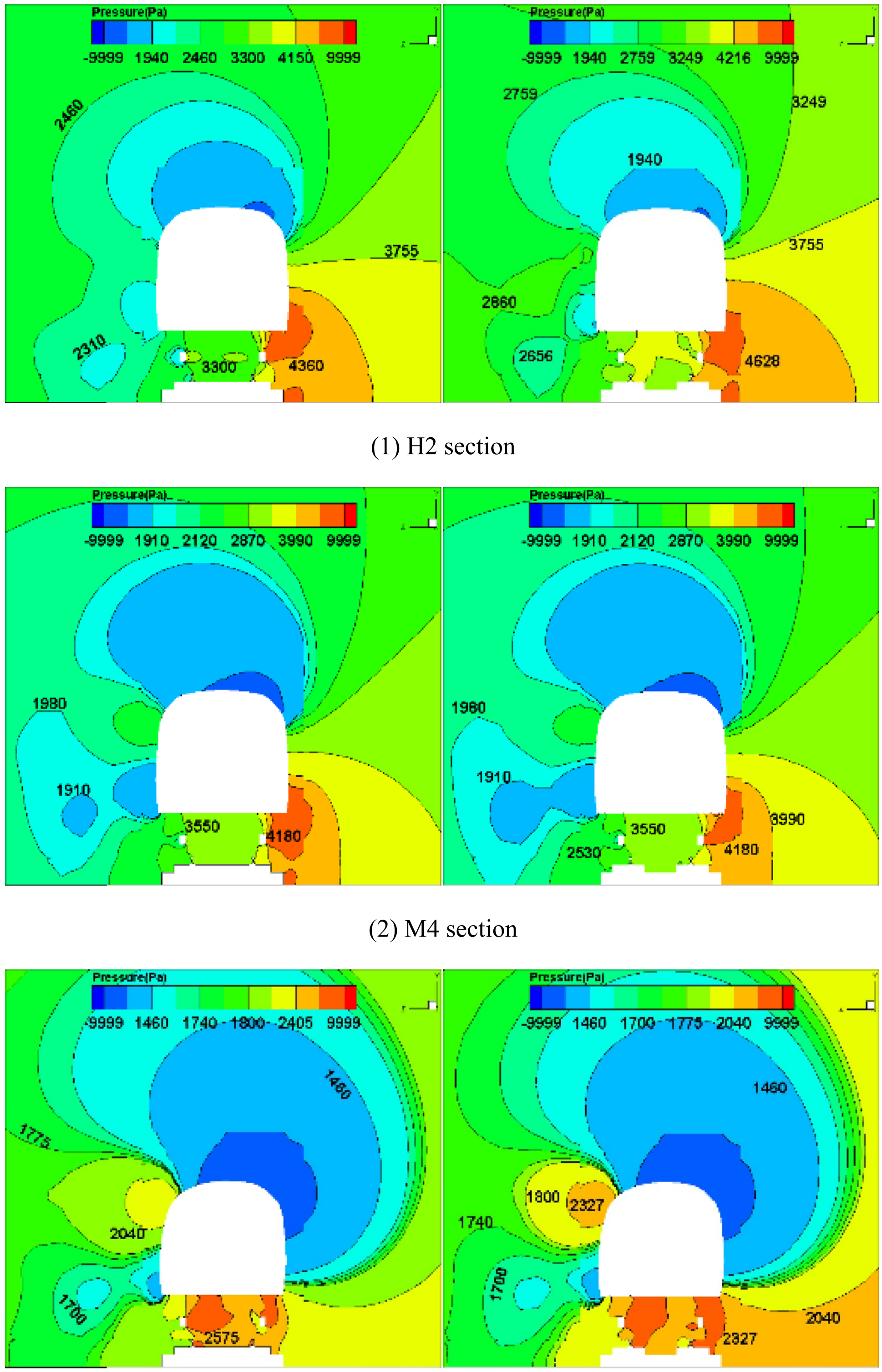

(1) H2 section

(2) M4 section

(3) T6 section

(a) Flat type (b) Frame type

3.6 The Influence of the Ballastless Track Structure on the Flow Field Distribution Around the Train Under a Crosswind

From the analysis of the pressure distribution in the previous section, the pressure changes are mainly concentrated on the bogie under the car, and the flow field analysis is also mainly concentrated on the flow field changes of the bogie under the car [33]. We analyzed the difference in the influence of the two track structures on the train flow field. Since the pressure distributions of the three sections H1, M3, and T5 are basically the same, and there is little difference in flow field distribution, no comparison will be made. Only the flow field distribution of the other three sections will be compared and analyzed.

Figure 18 shows the flow field distributions at the H2, M4, and T6 sections of the two track structures under the crosswind. When there is a crosswind, the direction of the streamline flow is mainly the same as the wind direction. Compared with the flat track structure with the frame track, the flow field distribution around the car body and the bogie is basically the same. The main difference exists in the area between the rail and the frame, but there are vortices in all three sections. There is no significant difference in the vortex structure, indicating that the vortex structure is not a reason for the pressure change under the vehicle. However, the pressure distribution under the car is significantly different. The pressure under the head car increases at the H2 section, indicating that the flow rate under the car decreases. Due to the existence of the frame structure, the space under the vehicle has increased, resulting in a decrease in the airflow

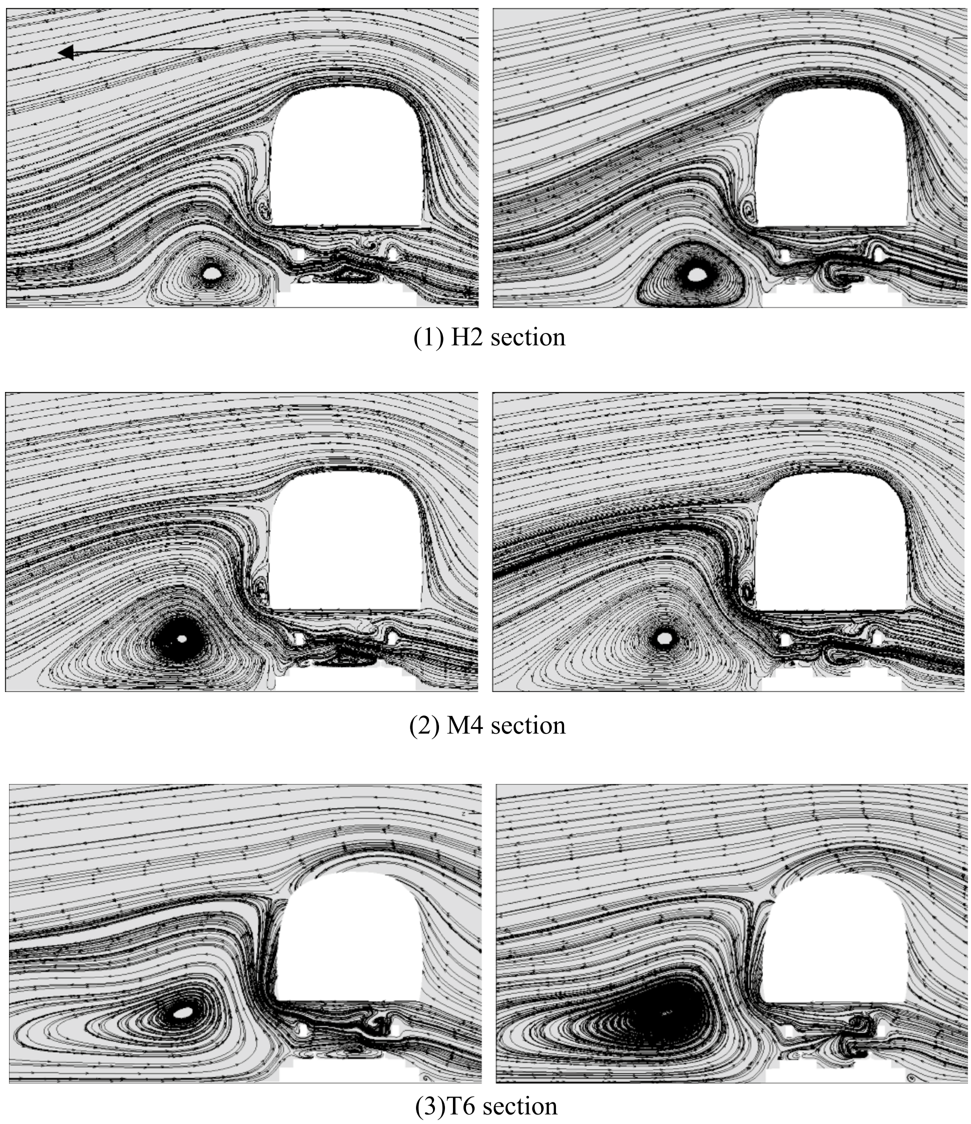

(a) Flat type (b) Frame type

Fig. 18 Flow field distribution at H2, M4, and T6 sections

rate and an increase in local pressure. At the T6 section, the pressure of the frame under the frame track drops, indicating that the crosswind speed under the frame type of the tail car is lower than that of the flat type. The crosswind speed of the tail car may be affected by many factors. Vortices tend to be created in the low-pressure area around the train. For example, there are low-pressure areas on both the leeward side and the lower left corner of the car body, which also generate vortices. Due to the rounded corner on the car body top, there are no vortices generated when the air flows over this smooth surface. At the bottom of the car body, due to the existence of complex structures such as bogies and rails, the fluid is blocked by obstacles, which generate vortices, and the pressure changes greatly.

From the above analysis, it can be seen that due to the coupling effect of the train wind and the crosswind, the wind speeds at different positions of the head, middle, and tail cars are significantly different. The wind speed of the head car is higher, and the tail car is smaller. The frame structure has a considerable influence on the aerodynamic characteristics of the train where the wind speed is high. The wind speed of the middle and tail cars is relatively stable and changes only slightly. From the difference in the distribution of train pressure and flow field in the same track structure under conditions of no natural wind and crosswind, it can be seen that the crosswind helps to stabilize the airflow around the train, and the vortex motion state will not be easily changed, resulting in smaller train aerodynamic changes than in the no natural wind environment.

4 Conclusion

In the present paper, the aerodynamic response, pressure, and flow field distribution of a high-speed train running on flat and frame ballastless tracks are analyzed under the action of no wind and different crosswind speeds (10, 15, 20, 25, and 30 m/s). The main research conclusions are as follows:

a. When there is no natural wind, compared with the flat track, the frame track causes the drag force of the whole vehicle to reduce; the maximum reduction percentage is only 2.15%, which is most affected by the drag force of the head vehicle. The increase in the whole vehicle lift force and the decrease in the lateral force are most affected by the middle car, resulting in a maximum increase of 12.5% in lift force and maximum decrease of 52.43% in lateral force. The frame track reduces the drag and lateral forces of the train but increases the lift force. Therefore, it is necessary to control the size of the frame in the actual engineering. High-speed rail operators can also consider using trains with a heavier body and wheel weights to run on the frame tracks.
b. The reason why the middle car has a greater influence on the lift and lateral forces is that the frame track structure changes the flow state of the airflow under the car, which changes the generation and dissipation opportunity of the vortex airflow of the back bogie under the head car. This effect continues to the front bogie of the middle car, making the front bogie of the middle car under the frame track more affected by the vortex dissipation, while the flat track is more affected by the vortex generation. Therefore, the direction of the two forces is changed, and the train aerodynamic force is also affected.
c. Compared with the flat track under the crosswind, the drag force of each car on the frame track is reduced, and the lift force of each car is increased. At a wind speed of 10 m/s, the lift force of the head and the tail vehicle is affected the most, increasing by 5.60 and 3.63%, respectively. The middle car is affected the most at a wind speed of 30 m/s, with an increase of 2.55%. The lateral force of the tail car increases greatly at a wind speed of 15 m/s, reaching 6.84%. Therefore, compared with the flat track, the safety of the tail car running on the frame track under a crosswind is worthy of more attention. In the area near the track, operators can consider installing windbreaks to reduce the crosswind impact. Due to the existence of the frame structure, the space under the vehicle increases, resulting in a decrease in the airflow and an increase in local pressure, which leads to changes in the train's aerodynamic force. Meanwhile, the train's aerodynamic change under the crosswind is smaller than that when there is no wind.

In the future, in order to improve the aerodynamic characteristics of trains on frame-type tracks, further studies are needed on the size and shape of the frame structure.

Acknowledgements The work described in this paper is supported by the National Natural Science Foundation of China (No. 11872136) and the Natural Science Foundation of Liaoning Province (No. 201602112). The authors are grateful to the anonymous reviewers for their constructive comments.

Funding The work described in this paper is supported by the National Natural Science Foundation of China (No. 11872136) and the Natural Science Foundation of Liaoning province (No. 201602112). The authors are grateful to the anonymous reviewers for their constructive comments. The funder had no role in the experimental design, model establishment, data analysis, manuscript writing, or decision to submit this article for publication.

Declarations

Conflict of interest The authors declare that they have no known competing financial interests or personal relationships that could have appeared to influence the work reported in this paper.

References

1. Xiao H, Zhang ZH, Chi YH, Wang XY, Wang HY, Jiang ZQ (2022) Structural analysis and parametric study ballasted track in sandy regions. Constr Build Mater 333:127439
2. Garcia J, Crespo A, Berasarte A et al (2011) Study of the flow between the train underbody and the ballast track. J Wind Eng Ind Aerod 99(10):1089–1098
3. Ding D (2017) High speed railway ballasted track aerodynamics research based on wind tunnel test and CFD simulation. MA. Eng dissertation, Beijing Jiaotong University
4. Zhang Y, Sun ZX, Yao YF, Liu W, Yang GW, Guo DL (2018) Influence of typical subgrade structures on aerodynamic characteristics of high speed trains in cross wind conditions. J Mech Eng 54(4):186–195
5. Li XZ, Wang M, Xiao J, Zou QY, Liu DJ (2018) Experimental study on aerodynamic characteristics of high-speed train on a truss bridge: a moving model test. J Wind Eng Ind Aerodyn 179:26–38
6. Baker CJ (2010) The simulation of unsteady aerodynamic cross wind forces on trains. J Wind Eng Ind Aerodyn 98:88–99
7. Gao C, Zhang JY, Li T, Sun Y (2020) Research on aerodynamic characteristics of front brake panel of high-speed train. Railw Stand Des 64(6):172–176
8. Li ZM, Li QL, Yang ZG (2022) Flow structure and far-field noise of high-speed train under ballast track. J Wind Eng Ind Aerodyn 220:104858
9. Song L, Liu HB, Cui CX, Yu ZW, Li ZG (2020) Thermal deformation and interfacial separation of a CRTS II slab ballastless track multilayer structure used in high-speed railways based on meteorological data. Constr Build Mater 237(C):117528
10. Chen M, Sun Yu, Shengyang Z, Wanming Z (2021) Dynamic performance comparison of different types of ballastless tracks using vehicle-track-subgrade coupled dynamics model. Eng Struct 249:113390
11. Zhang JW, Cai CB, Zhu SY, Wang MZ, He QL, Yang SF, Zhai WM (2022) Experimental investigation on dynamic performance evolution of double-block ballastless track under high-cycle train loads. Eng Struct 254:113872
12. Ramos A, Gomes Correia A, Calçada R, Connolly DP (2022) Ballastless railway track transition zones: an embankment to tunnel analysis. Transp Geotechn (prepublish):100728
13. Lin PZ, Wang YP, Li HM et al (2019) Coupling vibration characteristics of trains and subrail structures during high speed trains passing each other with same Speed. China Railw Sci 40(6):37–44
14. Chen L, Yao QL (2016) Numerical analysis on the influence of different ballastless tracks on vehicle dynamics. J East China Jiaotong Univ 33(4):1–9
15. Jiang HG, Li YX, Wang YJ, Yao K, Yao ZY, Xue ZC, Geng XY (2022) Dynamic performance evaluation of ballastless track in high-speed railways under subgrade differential settlement. Transp Geotech (prepublish):100721
16. Yang Y, Zhang GJ, Wu G, Cao DF (2022) Study on fatigue damage laws and life prediction of CRTS-II ballastless track slab. Eng Struct 252:113659
17. Zhao L, Zhou LY, Yu ZW et al (2021) Experimental study on CRTS II ballastless track-bridge structural system mechanical fatigue performance. Eng Struct 244:112784
18. Zhou LY, Zhao L et al (2021) Experimental study on stiffness degradation of Crts II ballastless track-bridge structural system under fatigue train load. Constr Build Mater 283:122794
19. Mao J, Xi YH, Yang GW (2012) Numerical analysis on the influence of train formation on the aerodynamic characteristics of high-speed trains under crosswind. China Railw Sci 33(1):78–85
20. Huang T, Li T, Zhang JY (2014) Effect of ballastless track on high-speed train aerodynamic characteristics. Chin Q Mech 35(4):604–614
21. Deng E, Yang WC, Lei MF, Zhu ZH, Zhang PP (2019) Aerodynamic loads and traffic safety of high-speed trains when passing through two windproof facilities under crosswind: a comparative study. Eng Struct 188:320–339
22. Xu G, Li H, Zhang J, Liang X (2019) Effect of two bogie cavity configurations on the underbody flow and near wake structures of a high-speed train. J Appl Fluid Mech 12(6):1945–1955
23. Li T, Zhang J, Rashidi M, Yu M (2019) On the Reynolds-averaged Navier–Stokes modelling of the flow around a simplified train in crosswinds. J Appl Fluid Mech 12(2):551–563
24. Xi YH (2012) Research on aerodynamic characteristics and running safety of high-speed trains under cross winds. Ph.D. dissertation, Beijing Jiaotong University
25. Mao J, Xi YH, Yang GW (2011) Research on influence of characteristics of cross wind field on aerodynamic performance of a high-speed train. J China Railw Soc 33(4):22–30
26. Liu ZC, Zhou D, Liang XF et al (2018) Research on aerodynamic characteristics of accelerating operation of high-speed train under wind environment. J China Railw Soc 40(7):40–46
27. Bell JR, Burton D (2016) Dynamics of trailing vortices in the wake of a generic high-speed train. J Fluidsand Struct 65:238–256
28. Xi YH, Mao J, Gao L et al (2015) Aerodynamic force/moment for high-speed train in crosswind field based on DES. J Central South University (Sci Technol) 46(3):1129–1139
29. Pan YC, Yao JW, Liang C et al (2017) Analysis on turbulence characteristics of vortex structure in near wake of high speed train. China Railw Sci 38(2):83–88
30. Bocciolone M, Cheli F, Corradi R (2008) Crosswind action on rail vehicles: wind tunnel experimental analyses. J Wind Eng Ind Aerodyn 96(5):584–610
31. Han YD, Yao S (2015) Real vehicle test and numerical simulation of flow field in high-speed train bogie cabin. J Traffic Transp Eng 15(6):51–60
32. Zhu JY, Hu ZW, Thompson DJ (2015) Analysis of aerodynamic and aeroacoustic behaviour of a simplified high-speed train bogie. Noise Vib Mitig Rail Transp Syst 37:489–496
33. Cai HM, Zhang JY, Li T (2018) Research on aerodynamic performance and flow field of high-speed train Bogie region. J Mech Eng 54(12):49–57